6-1-2005

Glycoprotein gp130 of *Dictyostelium discoideum* Influences Macropinocytosis and Adhesion

Catherine P. Chia
University of Nebraska - Lincoln, cchia1@unl.edu

Sujatha Gomathinayagam
University of Nebraska - Lincoln

Robert J. Schmaltz
University of Nebraska - Lincoln, rschmaltz2@unl.edu

Laura K. Smoyer
University of Nebraska - Lincoln, lsmoyer2@unl.edu

Molecular Biology of the Cell
Vol. 16, 2681–2693, June 2005

Glycoprotein gp130 of *Dictyostelium discoideum* Influences Macropinocytosis and Adhesion[D]

Catherine P. Chia, Sujatha Gomathinayagam, Robert J. Schmaltz, and Laura K. Smoyer

School of Biological Sciences, University of Nebraska–Lincoln, Lincoln, NE 68588-0118

Submitted June 12, 2004; Revised March 2, 2005; Accepted March 15, 2005
Monitoring Editor: Peter Devreotes

Glycoprotein gp130, found on the plasma membrane of *Dictyostelium discoideum* amoebae, was postulated previously to play a role in phagocytosis. The gene for gp130 was cloned and when translated, yielded a 768 amino acid preproprotein of 85.3 kDa. It had nearly 40% similarity to the 138 kDa family of glycoproteins implicated in sexual cell fusion during macrocyst formation in *D. discoideum*. The difference between the calculated size and observed M_r of 130 kDa on protein gels likely was due to N-glycosylation that was confirmed by lectin blots. Consistent with its surface-exposure, an antibody raised against recombinant protein stained the plasma membrane of *D. discoideum* amoebae. Gp130 and its transcripts were high during axenic growth of cells, but relatively low during growth on bacteria. The gene for gp130 was disrupted and cell lines lacking the glycoprotein were efficient phagocytes, indicating that gp130 was dispensable for phagocytosis. Gp130-null cells were similar in size to parent DH1 cells, had enhanced macropinocytosis and grew faster to higher densities. They also exhibited weaker cell-substrate adhesion but displayed greater cell-cell cohesion. Collectively, the data indicated that gp130 influenced macropinocytosis and played a role in adhesion during vegetative growth.

INTRODUCTION

The processes of phagocytosis, cell-cell and cell-substrate adhesion share a common initial event of recognition, whether it is of specific ligands or the chemical properties of the partner(s) in the interaction. With the long-term aim of understanding the mechanism of phagocytosis at the molecular level, particularly the early steps of recognition and binding, we have focused on surface-exposed molecules of the phagocytically active amoebae of *Dictyostelium discoideum*. *D. discoideum* cells are studied also for the related processes of motility and aggregation. When starved, individual but clonal cells coalesce into multicellular structures that, within a day, differentiate into fruiting bodies called sorocarps. Cell-cell recognition and adhesion are vital aspects of this developmental progression, and researchers have established that cell-surface molecules, including gp24 (Knecht *et al.*, 1987; Loomis, 1988; Brar and Siu, 1993), gp80 (Muller and Gerisch, 1978; Noegel *et al.*, 1986), and gp150 (Gao *et al.*, 1992; Wang *et al.*, 2000), are mediating these interactions (reviewed in Kessin, 2001 and Siu *et al.*, 2004). An understanding of the plasma membrane molecules involved in adhesive events during phagocytosis and motility of vegetative amoebae is emerging with the recent identification of cell-substrate adhesion molecule, sadA (Fey *et al.*, 2002) and the phg1 family of transmembrane 9 proteins (Cornillon *et al.*, 2000; Benghezal *et al.*, 2003).

This article was published online ahead of print in *MBC in Press* (http://www.molbiolcell.org/cgi/doi/10.1091/mbc.E04–06–0483) on March 23, 2005.

[D] The online version of this article contains supplemental material at *MBC Online* (http://www.molbiolcell.org).

Address correspondence to: Catherine P. Chia (cchia@unlserve.unl.edu).

In this study, we present evidence that a plasma membrane glycoprotein gp130 also played a role in cell-substrate adhesion during vegetative growth. Postulated to be a phagocytosis receptor (Chia, 1996), gp130 is possibly the same molecule as gp126, a surface-exposed glycoprotein suggested to have a dual role as both a phagocytosis receptor and a mediator of cell-cell cohesion (Chadwick and Garrod, 1983; Chadwick *et al.*, 1984; Chadwick, 1986). Characteristics of gp130 consistent with a role in phagocytosis are its presence in phagosomes, an association with detergent (Triton X-100)-insoluble cytoskeletons of bacterially grown cells but a depletion from membranes because of its internalization during phagocytosis (Chia, 1996; Rezabek *et al.*, 1997), and the presence of an altered form in a *D. discoideum* phagocytosis mutant (Vogel *et al.*, 1980). The relationship of gp126 to gp130 remains unresolved as the antibodies used for the studies on gp126 appeared to recognize carbohydrate rather than peptide epitopes. Antibodies raised against partially deglycosylated gp130 inhibited phagocytosis, but they too were not protein-specific as they recognized glycosylation modifications shared by *D. discoideum* glycoproteins (Chia and Luna, 1989). This finding supported the idea that carbohydrates could be partially responsible for cell-cell and cell-substrate interactions in *D. discoideum* but uncertainty remained regarding the function of gp130.

We report here the genomic sequence of the gene for gp130, expression patterns of the protein during growth and development, and biochemical and functional analyses of two transformed cell lines that specifically lack the protein. Gp130 was related to the family of gp138 proteins in *D. discoideum* that were postulated to participate in sexual cell fusion events leading to the formation of macrocysts (Aiba *et al.*, 1993; Fang *et al.*, 1993). As expected, gp130 was found at the cell-surface and expressed at high levels during vegetative growth of cells in axenic media. Protein levels were relatively low during growth on bacteria, a finding that

undercut an essential role for gp130 in phagocytosis. Cells with the gene for gp130 disrupted by the UMP synthase gene cassette were healthy, growing faster and to higher densities than parent cells. They also were competent in macropinocytosis and phagocytosis, and made normal but slightly smaller fruiting bodies. Compared with parent cells and consistent with its plasma membrane location, gp130-null cells had altered surface properties. They displayed weaker cell-substrate adhesion but paradoxically were more adhesive with each other. The complex phenotype of the gp130-null cells pointed to roles for gp130 in plasma membrane trafficking and cell-substrate adhesion.

Preliminary findings and the sequence of gp130 was presented in at the 40th Annual meeting of the American Society for Cell Biology (LaRosa *et al.*, 2000). The sequence is GenBank Accession No. AY038935.1 and also can be accessed through the *Dictyostelium* genome sequencing web site (http://www.dictybase.org) using DictyBase ID DDB0214937.

MATERIALS AND METHODS

Cell Growth and Development

Dictyostelium discoideum strains Ax2, Ax3, DH1 (Caterina *et al.*, 1994; in the presence of 20 μg/ml uracil), transformants 1C7 and 2F5 (this study), and gp138-null (Hata *et al.*, 2001; in the presence of 2 μg/ml blasticidin; Invitrogen, Carlsbad, CA) were grown at 22°C either axenically in HL5 medium (Watts and Ashworth, 1970) or in suspension with *Klebsiella aerogenes* as described (Chia, 1996) and shaken at 150 rpm. Cells were counted using a hemacytometer. Bacterial suspensions (inoculated with 1×10^5 *D. discoideum* cells/ml) were monitored using an OD600 of 1.0 corresponding to 1×10^9 bacteria/ml. Growth of cells on bacteria was unaffected by the inclusion or exclusion of uracil. For growth on lawns, *K. aerogenes* was grown overnight on SM plates at 37°C before inoculation with 1×10^5 *D. discoideum* cells (Sussman, 1987). Plates were put at 22°C and colony growth was measured daily. Three trials of growth were done, each with duplicates, and representative data are presented.

For starvation-induced development, cells were grown to midlog (5×10^6 cells/ml) before their collection by centrifugation. After two washes with Sorensen's buffer (SB; 14.6 mM KH_2PO_4, 2 mM Na_2HPO_4, pH 6.1), Resuspended cells (1×10^8 cells) were spread evenly on nonnutrient agar (1.5%) plates (100-mm diameter). Plates were stored in the dark and, over 24–36 h, images were recorded with a digital camera (Nikon Coolpix 995, Melville, NY) attached to a stereomicroscope (Nikon SMZ2800). Mounds, slugs, culminates, and fruiting bodies were counted at 12, 18, 24, and 36 h, respectively. For expression studies, cells scraped from plate surfaces were transferred to 1.5-ml microfuge tubes containing either 1 ml TRIzol reagent (Invitrogen, Carlsbad, CA) for RNA extraction or Laemmli sample buffer (Laemmli, 1970) containing 2 mM phenylmethylsulfonyl fluoride and a protease inhibitor mix (Roche Diagnostics, Indianapolis, IN) for protein analyses.

Nucleic Acid Analyses, Gene Disruption Construct and Transformation

A gene replacement vector was constructed by inserting the ~4-kb UMP synthase gene cassette containing the *Dictyostelium* pyr5-6 gene (DDPYR56G) into the unique *Cla*I site of the genomic sequence of gp130 cloned into pCR2.1 (Invitrogen). The cloning strategy used to acquire the gene for gp130 and details regarding its genomic sequence are described separately (Supplementary Data). The UMP synthase gene cassette had been released by digestion with *Cla*I from a gene replacement vector provided by Dr. M. Fechheimer (University of Georgia-Athens; Rivero *et al.*, 1996) and was originally derived from plasmid pJB1 (Jacquet *et al.*, 1988). The disrupted gp130 sequence was cut out of the pCR2.1 vector with sequential digestions using *Not*I and *Bam*HI, and used to transform DH1 cells by electroporation (Knecht and Pang, 1995). Transformants were selected by their growth in FM media (Qbiogene, Carlsbad, CA) in the absence of uracil and subcloned by limiting dilution. Two transformed cell lines, 1C7 and 2F5, were analyzed in parallel in the studies presented.

Genomic DNA was isolated from cultures of DH1, 1C7, and 2F5 grown in HL5 to densities of 6–10 $\times$ 10^6 cells/ml. Cells were harvested and lysed to obtain nuclei that (Myre and O'Day, 2002) were lysed with Buffer G2 (Blood and Cell culture DNA Maxi Kit; Qiagen, Valencia, CA), and the DNA was further purified following to the protocol provided by the vendor. Using standard molecular techniques (Sambrook and Russell, 2001) DNA was digested with restriction enzymes for 24 h at 37°, precipitated, loaded, and separated on 0.7% agarose gels that were blotted to positively charged nylon membranes (Roche Diagnostics). DNA was quantified with the Hoescht assay (Sambrook and Russell, 2001), using calf thymus DNA (Sigma, St. Louis, MO) as a standard.

Probes for Southern blots were prepared by PCR using digoxigenin-11-UTP (alkali-labile DIG; Roche) at one part of the DIG-UTP synthesis mix to three parts of the standard dNTP stock for the gp130-specific probe. The DIG-UTP synthesis mix was used without dilution for the DDPYR56G probe. Primers for the gp130-specific probe (1457 base pairs) were 5′- CAACGGACCCATGTTTAGATAAT (P1; forward) and 5′-ATCTTTACCTTTAATAGTAATAATAG-3′ (P2; reverse). Primers for the DDPYR56G probe (769 base pairs) were 5′-AGTAACAAGTGGTGCAAGTG-3′ (P3; forward) and 5′-ACCAACACACAAAGAACC-3′ (P4; reverse). The relative positions of primers P1–P4 are shown schematically in Figure 3A. Blots were processed according to the guidelines provided by Roche. Hybridization with the DDPYR56G-specific probe was at 42°C for 16 h. After exposure to film, blots were stripped according to Roche instructions and then hybridized with the gp130-specific probed at 37°C for 16 h. Exposures were 15 to 30 min.

Electrophoresis and capillary transfer of formaldehyde denaturing agarose gels for the separation of isolated RNA was performed according to standard protocols (Sambrook and Russell, 2001). Using the gp130 cDNA template, [α-^{32}P]dCTP was incorporated into DNA hybridization probes (1.3 kb) either by random priming using the Klenow fragment of DNA polymerase or gene specific primers and PCR. The blot was washed (each for 15 min at room temperature), first with 2$\times$ SSC, 0.1% SDS, followed by 0.5$\times$ SSC, 0.1% SDS, and then 0.2$\times$ SSC, 0.1% SDS and air-dried before exposure to film in the presence of intensifying screens.

Production of Bacterially Expressed Protein and Polyclonal Antiserum

After identifying a partial gp130 cDNA sequence, a translational fusion was constructed within the PQE-30 expression vector cassette (Qiagen) using *Bam*HI (AACTTGGATCCACATTTATTAATGTTCCAATTCCA) and *Hin*dIII (ATATGAAGCTTAGATAAAATGATTAATGATAATAA) adapter primers for the 5′ and 3′ ends, respectively. The construct was electroporated into *Escherichia coli* strain M15 containing the pREP4 plasmid. Screening of transformants, grown at 37°C, expressing the fusion protein initially was performed by colony hybridization with a ^{32}P labeled probes and later by immunoblotting using rabbit antibodies against a synthetic eight-residue peptide from gp130 (Chia, 1996). The fusion protein, predicted to have a molecular weight of 68.5 kDa, was comprised of an amino terminal sequence of MRGSHHHHHHGS followed by 609 amino acids (Thr151 to Ser759) of the conceptual preproprotein sequence derived from the cDNA. Restriction enzyme digests, PCR and cross-reactivity of the recombinant fusion protein to antipolyhistidine antibodies (His-probe H-15, Santa Cruz Biotechnology, Santa Cruz, CA) confirmed the production of the correct chimeric construct. Milligram quantities of the His-tagged protein were isolated and purified under denaturing conditions using nickel-nitrilotriacetic acid metal-affinity chromatography following vendor protocols (Qiagen). Antisera to the purified fusion protein were produced in rabbits at the Antibody Core Research Facility (Center for Biotechnology, University of Nebraska) following a standard immunization regime. An enriched IgG fraction that we call anti-gp130 was prepared from the antiserum by ammonium sulfate precipitation (Harlow and Lane, 1988) and used for detection of gp130 on protein blots.

Protein Analyses

Cells for lysates and plasma membrane preparations were harvested at densities between 6 and 9×10^6 cells/ml, unless otherwise noted in the figure legends. For lysates, cells were collected by centrifugation ($200 \times g$) and washed twice in SB before lysis in 0.5% SDS at 80°C. Plasma membranes (PMs), were prepared by filter lysis and sucrose density centrifugation (Das and Henderson, 1983) from axenically grown Ax2 or gp138-null cells kindly provided by Dr. Urushihara (University of Tsukuba, Japan; Hata *et al.*, 2001). Protein levels were measured using either the Bradford method (Bradford, 1976), after precipitating interfering SDS with 100 mM potassium phosphate, pH 7.2 (Zaman and Verwilghen 1979), or the Lowry method (Lowry *et al.*, 1951) in the presence of 0.1% SDS and bovine serum albumin (Pierce Chemical, Rockford, IL) as a standard.

SDS-PAGE was performed essentially as described (Laemmli, 1970). Gels electrophoretically transferred to nitrocellulose (Towbin *et al.*, 1979). Prestained markers (Benchmark, Invitrogen) were used to monitor electrophoresis. Blots were probed following standard protocols (Harlow and Lane, 1988) with antibodies followed by goat anti-rabbit or anti-mouse alkaline phosphatase conjugates (Southern Biotechnology Associates, Birmingham, AL). To detect glycoproteins, blots were probed with biotinylated concanavalin A (Con A; Biomeda, Foster City, CA) followed by streptavidin-alkaline phosphatase (Pierce Chemical; Chia, 1996). A previously described rabbit antibody was raised against a synthetic eight-residue peptide of gp130 (Chia, 1996). For this work, a different rabbit antibody (anti-gp130) was raised against bacterially expressed recombinant truncated version of gp130 (see above). Mouse monoclonal antibody AC11 reactive with gp138 was provided generously by Dr. Urushihara (Aiba *et al.*, 1993).

For immunolocalization, log-phase axenic cells were fixed and permeabilized at −10°C with 1% formaldehyde in methanol using the agar-overlay method (Fukui *et al.*, 1987). Slides were stained with or without anti-gp130 (75 μg/ml), followed by either FITC conjugated to goat anti-rabbit IgG (Sigma) adsorbed against glutaraldehyde-fixed Ax2 (Clarke *et al.*, 1987) or Cy2 donkey anti-rabbit conjugates (Jackson ImmunoResearch Laboratories, West Grove, PA). Coverslips were mounted in buffered Gelvatol containing 50 mg/ml 1,4-diazobicyclo-(2,2,2)-octane (Aldrich Chemical, Milwaukee, WI). Images were collected with a Bio-Rad MRC1024ES confocal laser-scanning microscope (Richmond, CA) at the University of Nebraska Center for Biotechnology Microscopy Core Facility.

Assays of Function

Fluid-phase Endocytosis, Exocytosis, and Phagocytosis. Macropinocytosis and exocytosis were measured with the fluid-phase marker FITC-dextran (M_r 70,000; Sigma; Seastone *et al.*, 2001). For endocytosis, cells in midlog phase were diluted with HL5 to 3×10^6 cells/ml and shaken with 2 mg/ml FITC dextran for 3 h. At various times cells were harvested, washed twice with SB, and then lysed with 0.5% Triton X-100 in SB. The fluorescence was measured with a Cary Eclipse spectrofluorimeter (Varian Instruments, Walnut Creek, CA) using 492 and 525 nm as the excitation and emission wavelengths, respectively. Duplicate samples of all cells were run in at least two trials of each assay. Live cells were imaged with an Olympus FluoView 500 (Olympus, Melville, NY) laser scanning microscope equipped with a 60× water immersion objective lens. Volumes of cell pellets were determined by centrifuging (2, 5, or 10×10^6) cells into calibrated micro-(capillary) pipettes. For exocytosis, cells in midlog phase were diluted with HL5 media to 3×10^6 cells/ml and loaded with 2 mg/ml FITC-dextran for 3 h. Cells then were washed twice with cold HL5 and resuspended in fresh HL5 without FITC-dextran. At times over a 3-h period, cells were harvested, washed twice with cold SB, and lysed with 0.5% Triton X-100 in SB, and their fluorescence was determined. To calculate the percent of fluorescence remaining in the cells, the fluorescence value at each time point was compared with the initial fluorescence, which was assigned a value of 100%. Phagocytosis was measured using Ds-Red fluorescent *E. coli* (Maselli *et al.*, 2002).

Motility and Adhesion

Cells in midlog phase were diluted with HL5 to 3×10^6 cells/ml, and 300 μl was placed in each well of an eight-well chambered slide (LabTek, Nagle Nunc International, Naperville, IL). For starved cells, midlog phase cells were harvested, washed twice with cold SB, and resuspended to 3×10^6 cells/ml, and 300 μl was left in a well for 5 h before recording images (Yuen *et al.*, 1995). An inverted microscope (Nikon Diaphot-TMD) equipped with Hoffman Modulation Contrast optics (40× objective; Modulation Optics, Greenvale, NY), camera (model DC-330 CCD; DAGE-MTI, Michigan City, IN) and CG-7 frame grabber (Scion, Frederick, MD) was used to collect video images at 1 frame/s in QuickTime 6.03. Three hundred frames were recorded and cell movement was measured by marking the position of the center of 25 cells every 60 frames. The total distance the cell traveled over a 5 min was determined and converted after determining the magnification using a micrometer scale observed with the same lens.

Cell-cell adhesion was assayed using a method previously described (Desbarats *et al.*, 1994). Midlog phase cells were collected and diluted to 3×10^6 cells/ml in HL5 (vegetative conditions) or SB (starvation conditions) and shaken at 22°C. At times indicated, 500 μl were transferred to a 1.5-ml microfuge tube, vortexed for 20 s, and mixed for 20 min using a Labquake shaker (Barnstead/Thermolyne C400110). Adhesion was measured by counting the number of single cells, and the number of cells in aggregates with a hemacytometer at each time point. Doublets were counted as aggregated cells. For suspension-development trials, late log phase axenically grown cells were harvested, washed twice in SB, and then suspended to 1×10^7 cells/ml in 17 mM phosphate buffer (pH 6.4) ± 5 mM EDTA. Because of their documented behavior during suspension-development, Ax3 cells were used as control cells instead of DH1. Cells were rotated at 180 rpm on a platform shaker, and at indicated times, aliquots were diluted to 2×10^6 cells/ml in the same buffer. Unaggregated cells (singlets and doublets) were counted, and the percentage of aggregated cells was determined (Desbarats *et al.*, 1994).

Cell substrate adhesion was measured following Barondes *et al.* (1987). Cells in midlog phase (5×10^6 cells/ml) was collected and diluted to 1×10^6 cells/ml in HL5. One hundred microliters of cells were added to wells of a 96-well polystyrene plate (Corning 25801) and allowed to settle and attach at room temperature for 30 min. The wells were then completely filled with HL5 without disturbing attached cells, sealed with an adhesive plastic sheet, inverted, and centrifuged for 5 min at $300 \times g$ at room temperature in a rotor with swinging microplate holders. After draining unbound cells, 150 μl of 0.4% SDS in SB was added to adhering cells, and the plate was shaken on a plate shaker at 37°C for 15 min to ensure complete lysis. Then, 150 μl of undiluted Coomassie Protein Assay Reagent (Pierce Chemical) was added to each well, and the plate was again shaken for 15 min at 37°C. The absorbance at 595 nm was read on a VersaMax microplate reader (Molecular Devices, Sunnyvale, CA) running SoftMax ProVer 4.6. The percentage of cells remaining in the wells was calculated from a standard curve generated by determining the amount of protein of a known number of cells and lysed in parallel with the experimental samples. At least three separate sets of the assay were done, with each set having the two transformants and parent DH1 in duplicate on the same plate.

RESULTS

Gp130 Related to the gp138 Family

Through a reverse genetics strategy, we obtained the genomic sequence for gp130, a plasma membrane glycoprotein postulated to have role in phagocytosis (Chia, 1996). Seven unique peptide sequences acquired from proteolyzed, gel-purified gp130 were back-translated to generate oligonucleotides for PCR with different templates. Concurrently, a partial genomic clone containing two sequenced peptides was identified in the databases of the *D. discoideum* Sequencing Consortium. This genomic clone, together with products from PCR trials, primer walking and anchored PCR, yielded first a cDNA sequence and subsequently the full genomic sequence for gp130 (see Supplementary Data for details).

From the amino acid sequence deduced from the coding sequence (2307 bases; GenBank accession no. AY038935.1), the predicted precursor of gp130 has a mass of 85.3 kDa (Figure 1A). If the predicted loss of signal peptides both at the N-and C-termini is taken into account (see below), the mass of the mature protein would be 79.7 kDa, which is nearly 50 kDa less than the M_r of 130 kDa observed originally on SDS-polyacrylamide gradient gels (Chia, 1996). The disparity likely is due to N-glycosylation, detected previously (Chia, 1996) of some of the 15 asparagines found in the Asn-X-Ser/Thr sequence used to predict glycosylation (Bause, 1983). The added carbohydrate would increase the mass of the molecule and also could retard its migration in SDS-gels. Weak glycosylation sites (when X is D, W, or P) and a site (N232) in a sequenced peptide are not indicated. Eleven Cys residues were present in mature gp130 and the absence of reductant increased slightly its SDS-gel mobility compared with the reduced form (Schmaltz and Chia; unpublished data). The strong biotinylation of gp130 that demonstrated its cell-surface exposure (Chia, 1996) was attributable to the numerous lysines potentially available (39 in the mature protein), and perhaps amino sugars, to react with amine-directed modifying reagents.

Several lines of evidence support the assignment of the start methionine. First, with the extreme AT-rich character of the 5′ region of the gene, there was no other methionine in region that yielded the appropriate open reading frame matching the two microsequenced peptides in the first exon. Second, gp130 showed significant similarity to the gp138 family of plasma membrane glycoproteins (see below; Fang *et al.*, 1993; Aiba *et al.*, 1997; Hata *et al.*, 2001). When the protein sequence of gp130 was aligned with the gp138 proteins using ClustalW (unpublished data; Thompson *et al.*, 1994; Accelrys, 2001), the position of the initial methionine of gp130 corresponded closely to the N-termini of the gp138 precursor proteins. Finally, using the assigned methionine, analyses of the preproprotein predicted a signal peptide (SPScan; Accelrys, 2001; and SignalP V1.1; Nielsen *et al.*, 1997), consistent with the biosynthesis of gp130 via the secretory pathway and its location at the plasma membrane (Chia, 1996). Attempts to acquire an N-terminal sequence of gel-purified gp130 were unsuccessful as it appeared blocked, so the first residue of the mature protein could not be verified.

Prediction programs for protein secondary structure indicated two major hydrophobic stretches of gp130 that could be embedded in the membrane and identified several addi-

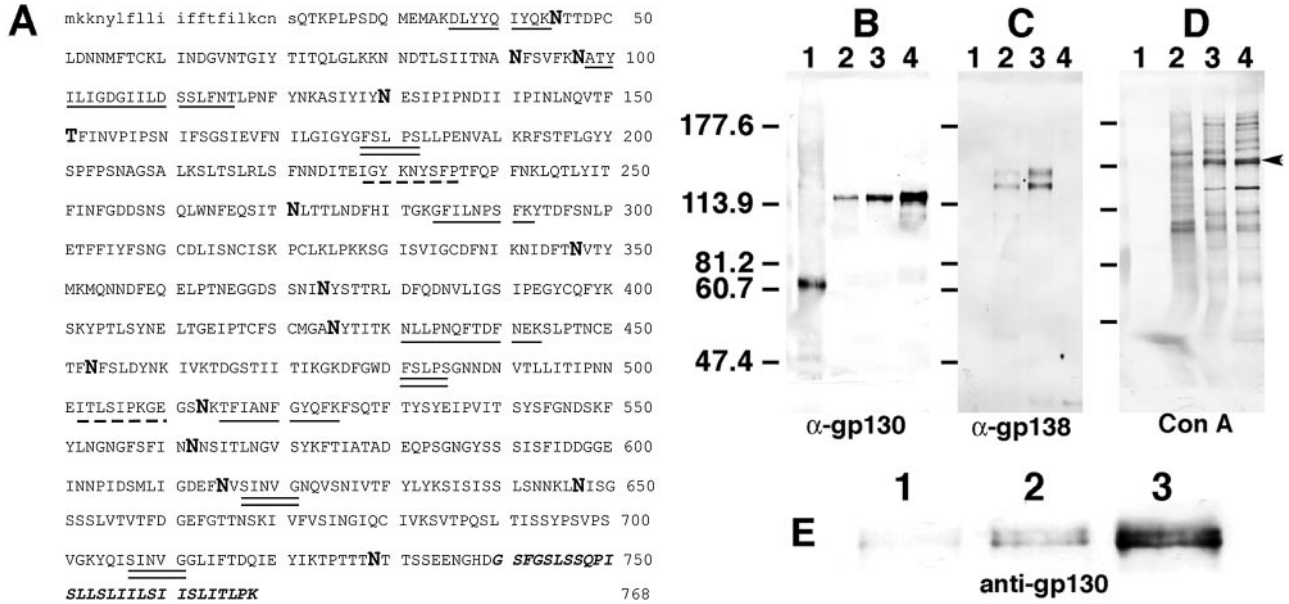

Figure 1. (A) Features of the deduced amino acid sequence of unprocessed gp130. The putative N-terminal signal peptide of 21 residues is in lower case. A bold N indicates potential N-linked glycosylation sites with the motif NX(T, S)X. A His-tag was fused to Thr151 (**T**) to produce a recombinant, truncated form of the protein. Microsequenced internal peptides from tryptic and endoproteinase Glu-C fragments are underlined with solid and dashed lines, respectively. Two peptides that are repeated (FSLPS; residues 178–182 and 481–485 and SINVG; residues 617–621 and 706–711) are underscored with double lines. Either Asp739 or Ser741 was predicted as the ω site, the C-terminal residue of the processed protein, after cleavage and attachment of a GPI-anchor. The cleaved C-terminal signal peptide (29 residues) is shown in bold italics if Asp739 is the ω site. (B–E) Reactivity of anti-gp130 with a plasma membrane glycoprotein. (B–D) Protein blots (of 8% polyacrylamide SDS-gels) that each has purified (bacterially expressed) recombinant protein that was injected into rabbits to produce anti-gp130 (lane 1), Ax2 lysate (lane 2), and plasma membranes from Ax2 (lane 3), and the gp138-null strain (lane 4). (E) Only the gp130 signal of Ax2 lysate (lane 1) and plasma membranes of Ax2 (lane 2) and a gp138-null strain (lane 3). Probes were anti-gp130 (4 μg/ml; B and E), monoclonal AC11 anti-gp138 (4 μg/ml; C) or biotinylated Con A (10 μg/ml; D). (A) Protein loads were as follows: 50 ng recombinant protein (lane 1); 2.5×10^4 cells (lane 2); 4 μg (lane 3), and 6 μg of membrane protein (lane 4). Relative to panel B, C and D had twofold more protein loaded, whereas E had one-half the protein loaded, per lane. Arrowhead in D indicates gp130. Positions of prestained size markers (kDa) are indicated to the left of C and D.

tional weakly hydrophobic short, internal segments. The possible membrane domains correspond to an N-terminal signal peptide of 21 residues and a 29-residue sequence at the C-terminus (Accelrys, 2001). No other transmembrane regions were predicted by the transmembrane hidden Markov model (TMHMM) routine (http://www.cbs.dtu.dk/services/TMHMM; Krogh *et al.*, 2001). PSORT, a program to analyze protein localization, also predicts a 21-residue signal peptide (Nakai and Kanehisa, 1992). Similarly, the "big-II" routines (http://mendel.imp.univie.ac.at/gpi/gpi_server.html; Eisenhaber *et al.*, 2000, 2001) indicated only two hydrophobic regions long enough to span a membrane. These correspond again to a signal peptide of 21 amino acids and the extremely hydrophobic 29-residue C-terminal sequence. The latter was predicted to direct the addition of a glycosylphosphatidylinositol (GPI) anchor. Previously, gp130 was postulated to be an intrinsic membrane protein, on the basis of its enrichment in purified plasma membrane fractions and a requirement of detergents for its solubility (Chia, 1996; Rezabek *et al.*, 1997). A protein with a GPI-anchor would have similar properties. Other than two repeated peptides (FSLPS and SINVG), no other notable features or credible motifs in the protein were detected using various gene and protein analysis programs.

Southern blot hybridization patterns were consistent with a single copy of the gene for gp130 (unpublished data). This finding was confirmed by BLAST searches of the *Dictyostelium* genome sequence databases that revealed a single copy of the gene. There was however significant sequence similarity of gp130 to the *D. discoideum* gp138 family of cell-surface glycoproteins postulated to mediate sexual cell fusion (Fang *et al.*, 1993; Aiba *et al.*, 1997), although questions have been raised regarding this function (Hata *et al.*, 2001). The gp138 genes map to chromosome 5 (Hata *et al.*, 2001), whereas the gp130 gene is on chromosome 3. Pairwise comparisons, using BESTFIT and GAP (Accelrys, 2001) show that the four gp138 proteins were much more similar to each other (82–87% similarity and 77–85% identity) than to gp130. Comparison of gp130 to each of the gp138 proteins showed it to have 40–42% similarity and 34–35% identity with the group. Thus, gp130 is related to the family of gp138 proteins, and the five proteins together comprise a distinct group in *D. discoideum* with no known relatives in other eukaryotes.

Expression and Localization of gp130

The sequenced gene was verified to encode for gp130 when polyclonal antibodies, generated against a truncated version of gp130, reacted strongly with the recombinant protein and specifically with gp130 (Figure 1). The recombinant protein used as the antigen migrated at 65 kDa, close to its predicted molecular mass of 68.5 kDa (Figure 1B, lane 1). Gp130 appeared as two closely spaced species in lysates of vegetative cells (Figure 1B, lane 2). As expected, a strong signal for gp130 was present in purified plasma membranes prepared from log-phase Ax2 and gp138-null cells (Figure 1B, lanes 3 and 4). The gp130 doublet in plasma membranes was more

evident with reduced protein loads (Figure 1E, lanes 2 and 3) and may be due to glycosylation differences. Anti-gp130 did not cross-react with gp138. The anti-gp130 signal in plasma membranes from gp138-null cells (Figure 1B, lane 4) migrated faster than anti-gp138 signals in Ax2 lysates and membranes (Figure 1C, lanes 2 and 3). The recombinant protein did not bind Con A, whereas the gp130 signals of lysates and plasma membranes corresponded to species that bound Con A (Figure 1D), indicating them to be glycoproteins. This observation supported the idea that glycosylation could account both for the doublet gp130 species and the slower mobility of the authentic protein. Deglycosylation of gp130 in plasma membranes using commercially available reagents was only partially effective, as judged by Con A blots of the treated plasma membranes (unpublished data). The reagents may have limited access to the glycosylated residues or the nature of the oligosaccharide modifications made them resistant to the treatments.

Gp130 was localized to the plasma membrane of axenically grown Ax2 cells stained with anti-gp130 as shown by the nearly exclusive staining of cell edges in confocal micrographs of fixed and permeabilized cells (Figure 2). This observation reinforced biochemical studies that showed gp130 to be readily surface-labeled with impermeant cell-labeling reagents and therefore found at the cell surface, and highly enriched in purified plasma membranes (Chia, 1996). Anti-gp130 reacted neither with native protein in plasma membranes nor Triton X-100–solubilized gp130 (as judged by ELISA analyses; unpublished data). It also did not bind to live cells, precluding its use in assays of live cells. The inability of anti-gp130 to react to native protein was expected since bacterially expressed protein was used as the antigen. Another contributing factor that could hinder its reactivity is that the polypeptide backbone of gp130 is masked by carbohydrate modifications, which were likely to be substantial based on the retarded mobility of gp130 on SDS-gels.

Northern blots of RNA derived from axenically grown cells showed a single transcript for gp130 of ~2.5 kb (Figure 2B). Levels of mRNA were high during vegetative growth and decreased during starvation-induced development. This pattern correlated well with the strong gp130 protein signal detected during (axenic) vegetative growth, whereas during development protein levels declined (Figure 2B). The lower levels of gp130 during development when cells are phagocytically inactive were consistent with the previous suggestion of a role for gp130 in phagocytosis (Chia, 1996; Rezabek *et al.*, 1997). Unexpected, however, was the observation that during growth phase, levels of gp130 were lower in bacterially grown cells compared with axenically grown cells (Figure 2C, top). The loss of protein was reflected in the northern blots showing reduced mRNA levels in phagocytically active cells compared with cells grown in nutrient media (Figure 2C, bottom). An examination of gp130 levels by immunoblotting in *D. discoideum* strain NC4 also showed only modest levels of gp130 (unpublished data). These expression patterns of gp130 during vegetative growth indicated that the relative amount of gp130 was inversely correlated with the phagocytic activity of cells.

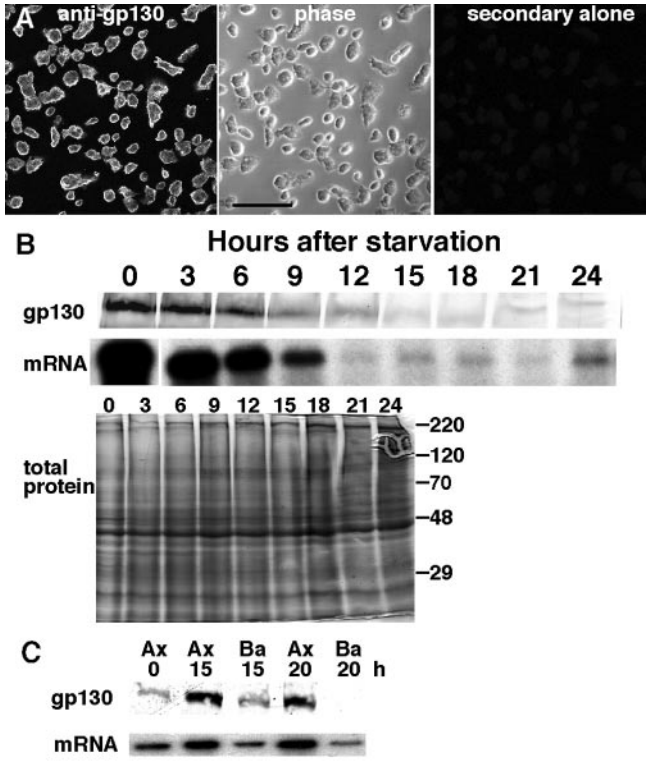

Figure 2. Localization and expression patterns of gp130. (A) Immunolocalization of gp130 in fixed and permeabilized, axenically grown Ax2. Cells stained with anti-gp130 (20 μg/ml) followed by FITC-labeled sheep anti-rabbit. The middle panel shows the phase image of the same field of cells, and the right panel shows cells stained with the secondary antibody alone. Scale bar, 50 μm. (B) Levels of gp130 mRNA and protein were high in vegetative cells and reduced during starvation-induced development. Top: immunoblot probed with anti-gp130. Twenty micrograms of total cell protein were loaded per lane of an SDS (10%) polyacrylamide gel. Middle: Northern blot with total RNA isolated from developed cells at times indicated probed with a ^{32}P-labeled probe specific for the gene for gp130. Ten micrograms of total RNA were loaded per lane of a 0.8% agarose gel. Bottom: SDS-gel, identical to the gel used for the immunoblot, stained with Coomassie blue to show equal protein loads. Positions of prestained size markers (kDa) are indicated to the right. (C) Axenically grown Ax2 contained more gp130 and its transcript than bacterially grown cells. Axenically growing cells were transferred from HL5 to fresh medium (Ax) or to a suspension of bacteria, washed, and resuspended in Sorensen's buffer (Ba; OD_{600} = 6). The time elapsed after the transfer is indicated in hours (h). Data are from a representative experiment. Top: immunoblot of a 10% SDS-gel (20 μg total cell protein loaded per lane) of axenically or bacterially grown Ax2 probed with anti-gp130. Bottom: levels of the mRNA for gp130 similarly were higher in axenically grown Ax2 compared with bacterially grown cells as judged by a Northern blot probed with a gp130-specific probe. Five micrograms of total RNA were loaded per lane of a 1.2% agarose gel.

Disruption of the Gene for gp130

DH1 cells, auxotrophic for uracil (Caterina *et al.*, 1994), were transformed with a construct where the UMP synthase gene cassette (Jacquet *et al.*, 1988) was inserted into the genomic sequence of gp130 (Figure 3A). Transformed cells were selected by their ability to grow in FM without uracil. Southern blots of genomic DNA from transformants 1C7 and 2F5 were probed with either gp130-specific or UMP synthase-specific probes. The hybridization patterns were consistent with a specific disruption of the genomic gene for gp130 with the cassette (Figure 3B).

Immunoblot analyses also showed the absence of gp130 in the transformants (Figure 3C). A signal for gp130 was present in DH1 cell lysates and plasma membranes (PMs; lane 1 in panels i–iii) but missing in 1C7 and 2F5 (lanes 2 and 4, respectively, in panels i–iii). For comparison, the gp138-null cell line was analyzed in parallel. As shown in Figure

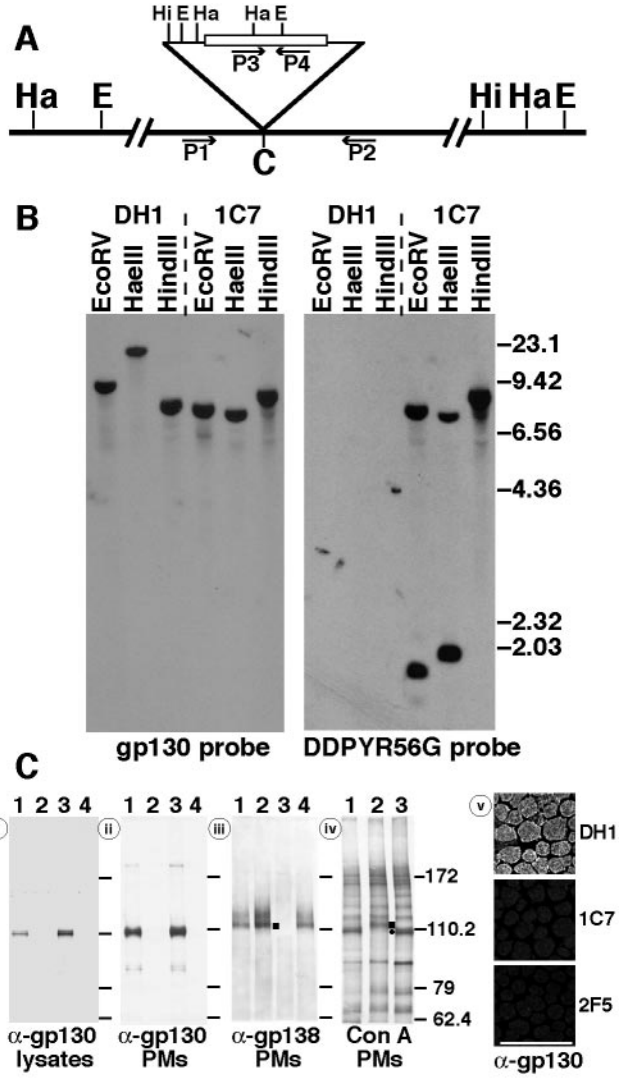

Figure 3. Evidence for a disrupted gene for gp130 and the absence of gp130 in transformants. (A) Schematic of contig JCa07f09 with a disrupted gene of gp130. The UMP synthase gene cassette (~4 kb) containing DDPYR56G (white rectangle) was inserted into the unique *Cla*I (C) site of the genomic sequence of gp130. Digoxigenin–labeled probes prepared by PCR using the primers indicated were specific for either gp130 (primers P1 and P2) or DDPYR56G (primers P3 and P4; see *Materials and Methods*). Restriction sites are indicated for the enzymes *Hae*III (Ha), *Hin*dIII (Hi), and *Eco*RV (E) in the UMP synthase cassette containing DDPYR56G and the 5′ (~18 kb) and 3′ (~9 kb) sequences (from contig JCa07f09) flanking the gene for gp130. (B) Southern blots of genomic DNA from transformant 1C7 indicated a disruption of the gene for gp130. Genomic DNA (5 μg per lane) was cut with the restriction enzymes indicated. The left panel shows the signals from a gp130-specific probe. The right panel shows the signals of the identical blot after it was stripped and probed with a DDPYR56G-specific probe. Dig II DNA size markers (kb; Roche) are indicated on the right. Transformants 1C7 and 2F5 had identical patterns but only 1C7 is shown. (C) Transformed cell lines 2F5 and 1C7 lack gp130. (i) Blot of lysates (10^5 cells/lane) from strains DH1 (lane 1), 2F5 (lane 2), gp138-null (lane 3), and 1C7 probed with anti-gp130. (ii) Blot of plasma membranes (PMs; 2 μg membrane protein/lane) probed with rabbit anti-gp130. Lanes are the same as panel i. (iii) Blot of plasma membranes (PMs; 4 μg membrane protein/lane) probed with mouse anti-gp138 AC11 (4 μg/ml). Lanes are the same as panel i. The black square corresponds to the Con A signal present in mutant 2F5 shown in panel iv. (iv) Blot of plasma membrane (PMs; 3 μg membrane protein/lane) probed with biotin Con A (10 μg/ml). Lanes are the same as panel i, except 1C7 is not shown. The black square indicates the species corresponding to the gp138 immunoreactive signal in panel iii and the black circle indicates the species corresponding to gp130. Positions of prestained markers (kDa) are indicated to the right of each blot. (v) Confocal micrographs show that unlike the parental cell line DH1, transformed cell lines 1C7 and 2F5 from log-phase cultures lack a plasma membrane signal when stained with anti-gp130 followed by a Cy2-donkey anti-rabbit conjugate. Scale bar, 50 μm.

1C, these cells lack two gp138 signals immunoreactive with monoclonal AC11 (Aiba *et al.*, 1993) that were present in PMs of DH1, 1C7, and 2F5 (panel iii). The Con A binding pattern of PMs from DH1, 2F5, and gp138 null cells showed the absence of a species corresponding to gp130 in 2F5 (panel iv, black circle). Also, compared with the parent DH1, there appeared to be an enhanced gp138 signal in 2F5 (lane 2, panel iii). This aligned with a Con A binding species present in PMs of 2F5, but absent in DH1 and gp138 null cells (panel iv, black square). Corroborating the lack of gp130 in PMs of the transformants, immunofluorescence microscopy showed 1C7 and 2F5 without the cell surface signal seen in DH1 cells (panel v). Together, the DNA and protein analyses support the conclusion that 1C7 and 2F5 were genuine transformants in which the gene for gp130 was disrupted.

Consequences of Disrupting the Gene for gp130

Growth and Development

The growth of the gp130-null cells appeared superior to DH1 both in suspension and on lawns of bacteria (Figure 4). In comparison to DH1 (generation time, GT, of 9 h), 1C7 and 2F5 grew faster (GT of 7–8 h) and reached higher densities in HL5 before reaching stationary phase (Figure 4A). Similarly, 1C7 and 2F5 exhibited faster growth rates (GT = 5 h) and achieved greater densities than DH1 (GT = 5.5 h) when grown in bacterial suspensions (Figure 4B). Neither the presence nor absence of uracil in DH1 suspension cultures had an effect on its growth (unpublished data). It seemed unlikely that gp130 was a receptor for specific nutrients present in HL5 because bacteria also were ingested at more rapid rates by the transformants. Both 1C7 and 2F5 also exceeded DH1 in terms of rate and overall size of colony growth on lawns of bacteria (Figure 4C). In addition, the clear zones of colonies of transformants expanded continuously over a 10-d period, whereas those of DH1 expanded slowly and ceased growing after a week (Figure 4, D and E). The absence of the gp130 protein appeared to enhance aspects of vegetative growth of the transformants.

On starvation-induced development, 1C7 and 2F5 formed normal structures and generated sorocarps that looked like those of DH1 (Figure 5). One difference, however, was their slightly slower pace of development. For example, at 12 h, 100% of the structures in DH1 were mounds, whereas only 60–70% of the structures were defined mounds in 1C7. A second difference was that for the same number of cells plated, transformants consistently made 20–40% more structures than DH1 (Figure 5B). This was more noticeable during the early stages such as when slugs had formed (Figure 5A, top), and less apparent by the time terminal sorocarp structures were formed. There were consequently fewer cells per structure, which led subsequently to slightly smaller sorocarps (Figure 5A, bottom).

Membrane Properties

The faster axenic growth of the gp130-null cells raised the question of whether they had faster rates of macropinocy-

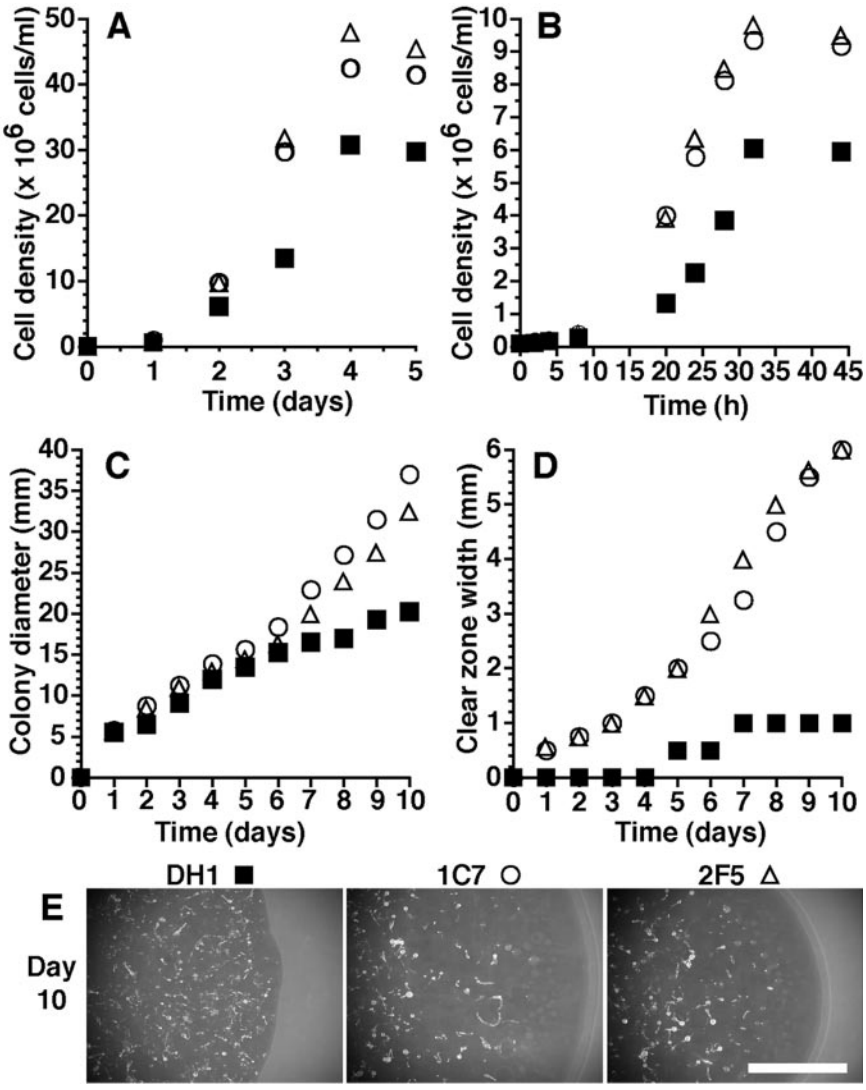

Figure 4. Transformed cell lines 1C7 and 2F5 had enhanced growth characteristics compared with parent DH1. (A) Transformants in HL5 grew faster and reached higher densities than DH1. (B) Transformants in bacterial suspensions grew faster and reached higher densities than DH1. (C) Colonies of the transformants grew faster on lawns of bacteria than parent DH1. (D) The clear zone of transformants expanded throughout colony growth, whereas that of the parent DH1 remained relatively constant. For all graphs: ■, DH1; ○, 1C7; △, 2F5. (E) Colonies of 1C7 and 2F5 after 10 d of growth on lawns of bacteria had larger clear zones than the colonies of DH1. Scale bar, 5 mm.

tosis. Both 1C7 and 2F5 took up FITC-dextran 2.5 times faster than that of DH1 cells during the initial 60 min of the assay where the rate was linear (Figure 6A). After 3 h, the fluorescence of 1C7 and 2F5 averaged 158% (±18%; two trials of each with duplicates) of DH1 cells. The faster growth rates in suspension cultures of the transformants thus could be attributed to their ability to take up nutrients more quickly than DH1 cells. Exocytosis by the mutants was typically slightly faster than DH1 but it was not statistically significant (Figure 6B). Vesicles containing FITC-dextran in the transformants appeared similar in size to those of DH1 after 1 h (Figure 6C) and 3 h (unpublished data). The transformants spread more quickly than DH1 cells when they settled on slides, making them seem significantly larger. Measurements of cell volumes, however, indicated that 1C7 and 2F5 were only 10–15% larger than DH1 cells. We conclude that the faster internalization of solute by 1C7 and 2F5, and not retarded exocytosis, accounted for their higher overall intracellular fluorescence. In contrast, particle uptake measured directly by phagocytosis of *E. coli*, by 1C7 and 2F5 was similar to that of DH1 (Figure 6D), consistent with the findings from the bacterial growth trials that gp130 was unessential for phagocytosis.

Another altered membrane property of the transformants was revealed by adhesion assays. Tests of cell-substrate adhesion using plastic (polystyrene) surfaces showed that gp130-null cells were nearly 50% less adherent to the plastic than DH1 cells (Figure 7A). The decreased cell-substrate adhesion did not, however, lead to greater motility, as the average velocity of vegetative 1C7 and 2F5 cells was close to that of DH1 (Figure 7B). The total distance traveled by the cells in a 5-min period and the patterns of cell movement were comparable (unpublished data). After 5 h in buffer (starvation), the three cell lines uniformly exhibited greater motile activity and moved similar distances (unpublished data).

When cell-cell adhesion was examined, log-phase 1C7 and 2F5 made 20–30% more aggregates in suspension in nutrient media (i.e., fewer single cells were present) than DH1 over time (Figure 7C). When vegetative cells of DH1, 1C7, and 2F5 were starved in SB, they all displayed rapid cell-cell adhesion within 1 h (Figure 7D). The tendency of 2F5 (and 1C7; unpublished data) to form more aggregates than DH1 was unaffected by the inclusion of EDTA (Figure 8A) or calcium (unpublished data). When starved for 1 h, disaggregated by pipetting and placed back in HL5, gp130-null cells

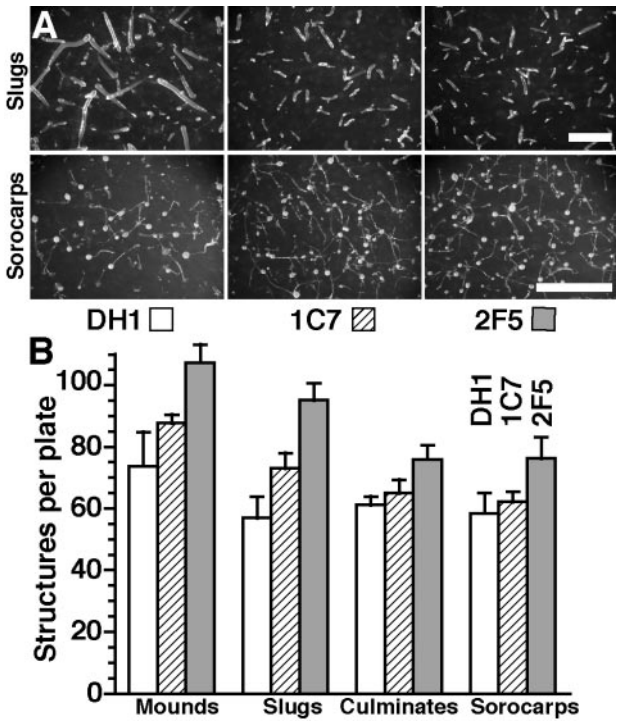

Figure 5. Transformed cells underwent development more slowly than DH1 but formed normal and more numerous structures. (A) Slugs (18 h) of transformants were smaller than those of DH1 (top row; scale bar, 2 mm), and consequently their sorocarps were smaller, but their morphology was like those of DH1 (bottom row; scale bar, 1 mm). (B) Although equivalent numbers of cells were plated, transformants formed more structures than DH1 during starvation-induced development. Open bar, DH1; cross-hatched bar, 1C7; gray bar, 2F5.

made more aggregates than DH1 cells that were similarly treated whether EDTA was absent or present (Figure 8B). Under the higher shear forces of shaken suspensions (180 rpm), starved 2F5 (and 1C7) formed more aggregates than control Ax3 cells (Figure 8C). The calcium-sensitive adhesion molecule gp24 (Brar and Siu, 1993) was likely responsible for the cohesion of the starved cells because 5 mM EDTA decreased the percentage of aggregates of 2F5 and Ax3. Under these conditions, however, gp130-null cells formed more aggregates than Ax3, raising the suggestion that the absence of gp130 revealed an EDTA-insensitive cell-cell adhesion mechanism during early development. Cell lysis occurred when transformants were shaken in buffer with EDTA for more than 5 h, so these studies did not go beyond 6 h.

In summary, compared with parent DH1 cells, gp130-null cell lines 1C7 and 2F5 during vegetative growth had increased fluid-phase endocytosis, enhanced cell-cell cohesiveness, and decreased cell-substrate adhesion, whereas phagocytosis and motility appeared similar. The altered cell-surface properties appeared due to the absence of gp130 on the plasma membrane and indicated that gp130 influenced how *D. discoideum* cells interacted with each other and other surfaces. Because expression patterns of normal cells indicated a depletion of gp130 during starvation and development, predictably, under these conditions, gp130-null cells on substrates behaved largely like DH1 cells.

DISCUSSION

Cloning and Expression of gp130

We have reported the cloning and sequencing of the gene for the glycoprotein gp130, suggested previously to have a role

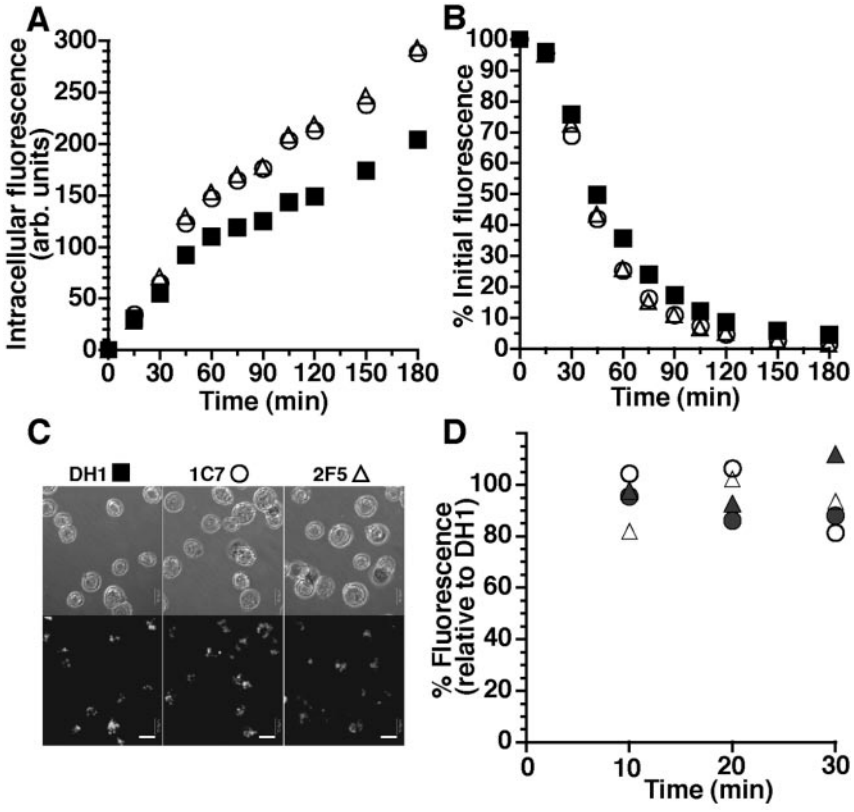

Figure 6. Gp130-null cells exhibited greater macropinocytosis activity than DH1 cells. (A) Fluid-phase endocytosis by 1C7, 2F5, and DH1. (B) Exocytosis of fluorescence by 1C7, 2F5, and DH1 loaded with FITC-dextran. For both graphs: ■, DH1; ○, 1C7; △, 2F5. (C) Live 1C7, 2F5, and DH1 cells loaded for 1 h with FITC-dextran showed their fluorescent vesicles to be similar in size. Scale bar, 10 μm. (D) Phagocytosis of *E. coli* by 1C7 and 1F5 was similar to that of DH1. Shown are two trials (open and filled symbols) where activity is expressed relative to DH1 (average of duplicates for each time point). Circles, 1C7; triangles, 2F5.

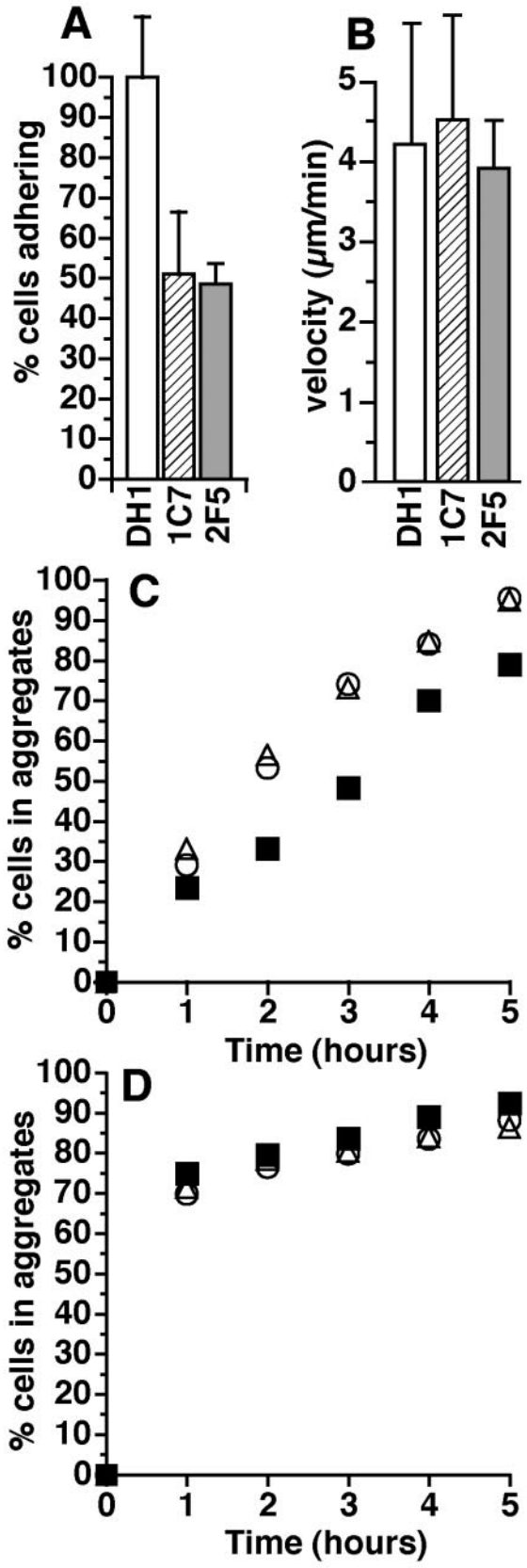

Figure 7. Altered adhesiveness of transformants during vegetative growth. (A) Log-phase transformants were less adherent to plastic than parent DH1. Open bar, DH1; cross-hatched bar, 1C7; gray bar, 2F5. (B) Motility of log-phase transformants was similar to DH1. For graphs A and B, open bar, DH1; cross-hatched bar, 1C7; gray bar, 2F5. Mean and SEM are indicated. (C) Log-phase transformants made more aggregates in suspension (HL5) than parent DH1. (D) Vegetative cells of 1C7, 2F5, and DH1 placed under starvation conditions in suspension showed similar adhesiveness. For graphs C and D: ■, DH1; ○, 1C7; △, 2F5.

in *D. discoideum* phagocytosis (Chia, 1996). The proper reading frame and positions of two introns were established by seven internal microsequenced peptides. Additional corroboration of the sequence was aided by the identification of the sequence in contigs later available through the databases of the *Dictyostelium* genome sequencing project (Supplementary Data Figure 1). The presence and relative abundance of gp130 in vegetative (log-phase) axenically grown cells and purified plasma membranes, and its uniform plasma membrane location were consistent with a phagocytic function (Figures 1 and 2A). The amount of gp130 protein and its transcript were, however, unexpectedly lower in bacterially grown cells than in axenically grown cells (Figure 2, B and C). This expression pattern was inconsistent with a vital involvement of gp130 in phagocytosis. Further, because null cells were efficient phagocytes (Figures 4B and 6D), the protein was dispensable for phagocytosis, although different particles and solution conditions were not tested.

Aside from an expected N-terminal signal sequence, a C-terminal hydrophobic sequence that might direct the addition of a GPI-anchor, and N-glycosylation motifs, conserved protein regions or patterns in gp130 were not evident nor did various programs (Bateman *et al.*, 2002; Hulo *et al.*, 2004) that predict protein secondary structure provide immediate insights into the function of gp130. Additionally, gp130 had no significant resemblance to proteins in the databases except for the gp138 family suggested to be involved in sexual cell fusion of *D. discoideum* (Fang *et al.*, 1993; Hata *et al.*, 1999), although a subsequent study raises doubts about this role (Hata *et al.*, 2001). The absence of relatives for gp130 and the gp138 group in other organisms suggests that these glycoproteins have unique roles in the biology of *D. discoideum*.

Function of gp130

Mutants lacking gp130 in *D. discoideum* were generated with the expectation that the cells would provide insights into the function of the protein. Southern blot analyses showed the gene for gp130 was disrupted, and immunoblots showed the corresponding absence of gp130 in transformants (Figure 3). Biochemical and physiological analyses indicated that cells lacking the protein had defects in neither growth nor developmental. Rather, gp130-null cells had faster growth rates and attained higher densities in nutrient HL5 media and bacterial suspensions, before reaching stationary phase, than the parent DH1 (Figure 4, A and B). The more robust growth of 1C7 and 2F5 in HL5 could be attributed to the higher activities of macropinocytosis (Figure 6A). Although particle uptake rates were similar for the cells when measured directly for short times (Figure 6D), growth of the gp130-null cells in bacterial suspensions was superior to DH1 (Figure 4B). The higher growth rates might be related to greater endocytotic activity that was more evident over time and consistent with the enhanced rates of fluid-phase uptake.

Studies of endocytosis in mammalian cell lines, yeast and *D. discoideum* commonly yield cases where macropinocytosis is disrupted rather than improved after gene mutations. For example, because the cytoskeleton plays a role in endocyto-

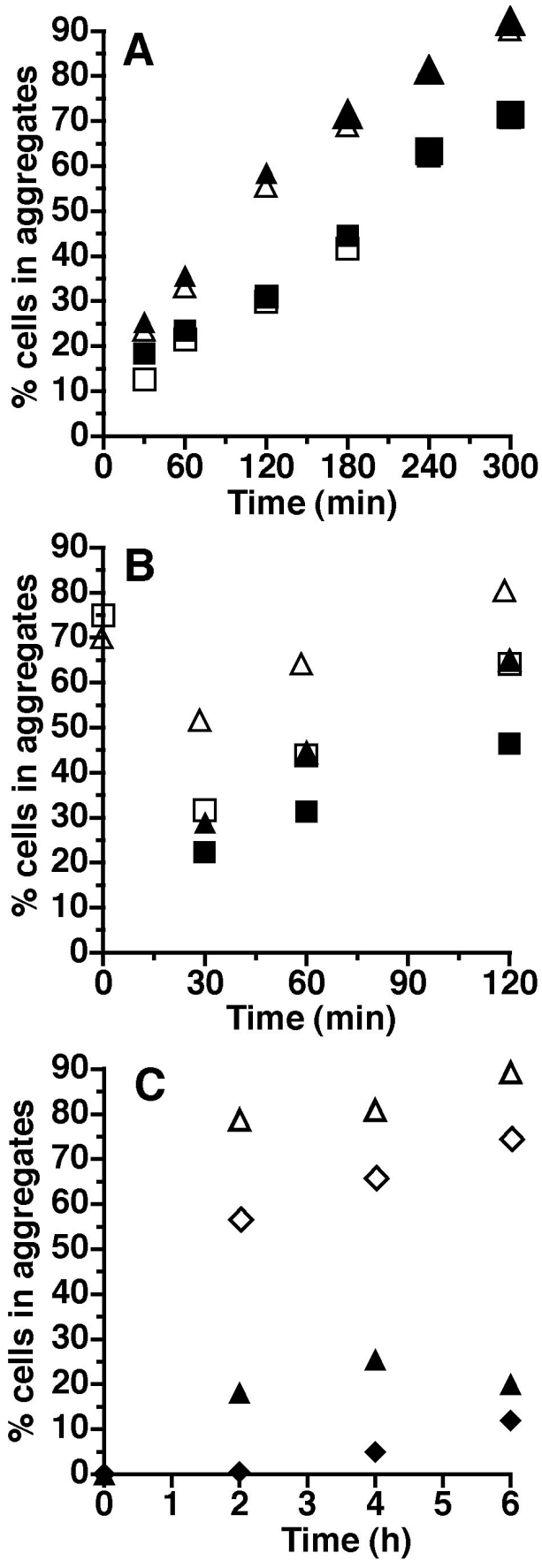

sis (Qualmann *et al.,* 2000; Qualmann and Kessels, 2002; Engqvist-Goldstein and Drubin, 2003), mutations in actin-binding proteins adversely affect macropinocytosis in *D. discoideum* (Maniak, 2001). A faster doubling time by *D. discoideum* cells lacking the substrate adhesion receptor sadA was due to the cytokinesis of multinucleate cells and not improved endocytosis (Fey *et al.,* 2002). It seems unlikely that the improved growth characteristics of the gp130-null cells were a consequence of the inserted UMP synthase gene because a number of cell lines with genes disrupted with this cassette display rates of endocytosis the same as or less than that of the DH1 parent cell line (Rivero *et al.,* 1996; Dragoi and O'Halloran, 1998; Liu *et al.,* 2002). The robust growth characteristics of gp130-null cells thus were unforeseen. We offer two explanations for the observed behaviors of the transformants. One is that because gp130 was a component of the plasma membrane, its absence caused changes in the physical nature of the membrane bilayer that led to greater endocytotic activity. A second related scenario is that gp130 was involved directly in a mechanism governing membrane recycling. Its absence led to elevated rates of membrane trafficking, with the consequence of increasing overall endocytotic activity. Because cytoskeletal-membrane interactions are vital for macropinocytosis, the relationship of gp130 to other membrane or cytoskeletal proteins is a focus of future studies.

Colony growth rates as well as the continued expansion of clear zones on bacterial lawns by the gp130-null cells pointed to their faster movement on surfaces (Figure 4, C and D). This was consistent with their altered membrane flux and their decreased cell-substrate adhesion (Figure 7A) because cell migration is closely linked to interactions between cell and substratum (Bray, 1992; DeMali and Burridge, 2003). However, the rate of movement of the cells in HL5 on glass slides was similar to that of DH1 (Figure 7B), and their patterns of movement appeared the same when comparing their paths. The larger colony sizes and clear zones may reflect simply the enhanced growth rates of gp130-null cells seen in suspension culture.

Alternatively, the nature of the substrate may influence the strength of the cell-substrate interaction. This could explain how the weaker cell-substrate adhesion of the gp130-null cells allowed them to be fully capable of phagocytosis, a localized cell-substrate adhesion event (May and Machesky, 2001). Typically, cell-substrate adhesion and phagocytic competence are highly correlated (Bray, 1992; May and Machesky, 2001; DeMali and Burridge, 2003). One example is the sadA-null cells unable to attach to plastic that are also phagocytically incompetent (Fey *et al.,* 2002). Likewise, *phg1* cells, generated by insertional mutagenesis, have defective

Figure 8. Increased formation of aggregates of gp130-null cells was EDTA-insensitive. Experiments included both transformants but only data for 2F5 are shown. (A) Aggregation of vegetative 2F5 in suspension (HL5) was greater than DH1 (open symbols, without EDTA), and unaffected by 5 mM EDTA (filled symbols). (B) Cells were starved for 1 h in Sorensen's buffer (SB) in the absence of EDTA, dispersed into individual cells by gentle pipetting, and allowed to reaggregate in HL5 without (open symbols) and with 5 mM EDTA (filled symbols). Transformant 2F5 reaggregated more than DH1 cells, even in the presence of 5 mM EDTA. For reference, % aggregates after 1 h in SB are plotted on the *y*-axis. (C) Cells were starved in SB ± 5 mM EDTA and rotated at 180 rpm on a platform shaker. During early starvation-induced (suspension) development, transformant 2F5 made more aggregates than Ax3 in the absence (open symbols) or presence (filled symbols) of EDTA. Symbols: boxes, DH1; triangles, 2F5; diamonds, Ax3.

phagocytosis that coincides with faulty adhesion (Cornillon *et al.*, 2000). Mutants of cortical cytoskeletal proteins such as talin (Niewöhner *et al.*, 1997) and myosin VII (Tuxworth *et al.*, 2001) similarly show a tight coupling of phagocytosis and adhesion. Because gp130-null cells had 50% of the cell-substrate adhesion of the parent DH1 cells, but were phagocytically functional, it appeared that gp130 participated in a cell-substrate adhesion mechanism different from the sadA and phg1 proteins, and also distinct from that used in the recognition of *Klebsiella aerogenes* and *E. coli* bacteria. We thus consider the idea that gp130 was a lectin-type receptor postulated by Vogel *et al.* (1980). Phagocytosis by the gp130-null cells could be performed by the "nonspecific" receptors that compensated for gp130 so its absence was not a liability. We also consider the possibility that gp130 was part of the cellular adhesion assemblage of surface molecules postulated to be controlled by the transmembrane 9 family of proteins Benghezal *et al.* (2003). Thus, gp130 could still have a role in phagocytosis as a specific receptor. Because the adhesion assay tested only cell interactions with plastic, the nature of a cell surface-adhesion system mediated by gp130 should be explored further by testing how cells ingest particles with different chemical properties under different conditions (Vogel *et al.*, 1980; Cornillon *et al.*, 2000).

Although the transformants exhibited weaker cell-substrate adhesion, it was paradoxical to find that compared with the cell-cell cohesion of DH1 cells, vegetative gp130-null cells were relatively more cohesive with each other in suspension (Figure 7C). Although cell-cohesion is typically not measured in vegetative cells, Marin *et al.* (1980) observed that nearly half the vegetative cells make aggregates (of three or more cells) within 30 min in a suspension of nutrient media.

The interaction of gp130-null cells was not wholly attributable to gp24, the molecule mediating calcium-dependent cell-cell cohesion during early development (Knecht *et al.*, 1987; Loomis, 1988; Brar and Siu, 1993), because neither EDTA (Figure 8A) nor calcium (unpublished data) reduced the cohesion of transformants from log-phase cultures. When dis-aggregated and returned to HL5, transformants exhibited stronger cohesion than DH1 (Figure 8B). Suspension-starved transformants under higher shear forces also made more aggregates than control cells (Figure 8C). A component of this aggregation was apparently mediated by gp24 as the inclusion of EDTA decreased the total percentage of transformants and Ax3 cells in aggregates. Transformants, however, maintained a greater number of EDTA-resistant aggregates than Ax3 cells. These observations indicate that cells had the ability to self-cohere, in an EDTA-insensitive manner, which became more evident when gp130 was absent. Although the effectiveness of EDTA in HL5 is unclear, the adhesion mechanism displayed by vegetative transformants (Figure 8A) and the EDTA-resistant self-cohesion in shaken suspension were likely related. Studies of gp24-null cells revealed a class of EDTA-sensitive cell adhesion sites (Wong *et al.*, 2002), although we do not know whether these are responsible for cohesive interactions of the vegetative transformants. Because gp130 contributed to substrate adhesion, a possibility is that its presence masked or suppressed cell-cell cohesion. Alternatively, the greater self-cohesion of transformants could be due to precocious expression of gp80, the EDTA-resistant cell-cell adhesion molecule. Desbarats *et al.* (1994) showed that cell-cell adhesion and contact are involved in the induction of gp80 expression.

The complex phenotype of gp130-null cells pointed to a role for gp130 in inhibiting cell-cell cohesion during vegetative growth while participating in cell-substrate adhesion when cells were in contact with dissimilar surfaces. Gp130-null cells also exhibited increased macropinocytosis, indicating that the absence of the glycoprotein enhanced membrane trafficking. We anticipate that analyses of cell lines that maintain or overexpress gp130 during development, or express fluorescently tagged gp130, will provide more details regarding its adhesion functions and impact on membrane flux.

ACKNOWLEDGMENTS

We thank Drs. Zhou and Hou for assistance with the acquisition of confocal microscopy images; Dr. G. Orti for use of the ABI sequencers; M. Fatemi, J. Keblesh, M. Meier, and P. C. LaRosa for technical assistance; Dr. Urushihara (U. Tsukuba, Japan) for gp138-null cells and anti-gp138 monoclonal antibody AC11; and Drs. Maselli and Knecht for DsRed-*E. coli*. C.P.C. thanks Drs. Fechheimer and Furukawa (Univ. Georgia-Athens) for their scientific advice and generosity. Blast searches of *Dictyostelium* sequences were performed through the National Biomedical Computation resource (NIHP41-RR80605) at the San Diego Supercomputer Center. The *Dictyostelium discoideum* Sequencing consortium was funded by the Deutsche Forschungsgemeinschaft, the National Institutes of Health, the Medical Research Council, and the European Union. This work was supported by National Science Foundation grants MCB-95133628 and MCB-0079967 to C.P.C. and the U. Nebraska Center for Biotechnology.

REFERENCES

Accelrys. (2001). Genetics Computer Group. Wisconsin Package Version 10.2.

Aiba, K., Fang, H., Yamaguchi, N., Tanaka, Y., and Urushihara, H. (1997). Isoforms of gp138, a cell-fusion related protein in *Dictyostelium discoideum.* J. Biochem. *121*, 238–243.

Aiba, K., Yanagisawa, K., and Urushihara, H. (1993). Distribution of gp138, a cell surface protein responsible for sexual cell fusion, among cellular slime moulds. J. Gen. Microbiol. *139*(Pt 2), 279–285.

Barondes, S. H., Cooper, D. N., and Springer, W. R. (1987). Discoidins I and II: endogenous lectins involved in cell-substratum adhesion and spore coat formation. Methods Cell Biol. *28*, 387–409.

Bateman, A., Birney, E., Cerruti, L., Durbin, R., Etwiller, L., Eddy, S. R., Griffiths-Jones, S., Howe, K. L., Marshall, M., and Sonnhammer, E. L. (2002). The Pfam protein families database. Nucleic Acids Res. *30*, 276–280.

Bause, E. (1983). Structural requirements of N-glycosylation of proteins. Studies with proline peptides as conformational probes. Biochem. J. *209*, 331–336.

Benghezal, M., Cornillon, S., Gebbie, L., Alibaud, L., Bruckert, F., Letourneur, F., and Cosson, P. (2003). Synergistic control of cellular adhesion by transmembrane 9 proteins. Mol. Biol. Cell *14*, 2890–2899.

Bradford, M. (1976). A rapid and sensitive method for the quantitation of microgram quantities of protein utilizing the principles of protein-dye binding. Anal. Biochem. *72*, 248–254.

Brar, S. K., and Siu, C.-H. (1993). Characterization of the cell adhesion molecule gp24 in *Dictyostelium discoideum.* J. Biol. Chem. *268*, 24902–24909.

Bray, D. (1992). Cell movements, New York: Garland.

Caterina, M. J., Milne, J. L., and Devreotes, P. N. (1994). Mutation of the third intracellular loop of the cAMP receptor, cAR1, of *Dictyostelium* yields mutants impaired in multiple signaling pathways. J. Biol. Chem. *269*, 1523–1532.

Chadwick, C. M. (1986). Changes in the cell surface level of gp126 during development of *Dictyostelium discoideum.* Devel. Growth Differ. *28*, 203–211.

Chadwick, C. M., Ellison, J. E., and Garrod, D. R. (1984). Dual role for *Dictyostelium* contact sites B in phagocytosis and developmental size regulation. Nature *307*, 646–647.

Chadwick, C. M., and Garrod, D. R. (1983). Identification of the cohesion molecule, contact sites B, of *Dictyostelium discoideum.* J. Cell Sci. *60*, 251–266.

Chia, C. P. (1996). A 130-kDa plasma membrane glycoprotein involved in *Dictyostelium* phagocytosis. Exp. Cell Res. *227*, 182–189.

Chia, C. P., and Luna, E. J. (1989). Phagocytosis in *Dictyostelium discoideum* is inhibited by antibodies directed primarily against common carbohydrate epitopes of a major cell-surface plasma membrane glycoprotein. Exp. Cell Res. *181*, 11–26.

Clarke, M., Kayman, S. C., and Riley, K. (1987). Density-dependent induction of discoidin-I synthesis in exponentially growing cells of *Dictyostelium discoideum.* Differentiation *34*, 79–87.

Cornillon, S., Pech, E., Benghezal, M., Ravanel, K., Gaynor, E., Letourneur, F., Bruckert, F., and Cosson, P. (2000). Phg1p is a nine-transmembrane protein superfamily member involved in *Dictyostelium* adhesion and phagocytosis. J. Biol. Chem. *275*, 34287–34292.

Das, O. P., and Henderson, E. J. (1983). A novel technique for gentle lysis of eukaryotic cells. Isolation of plasma membranes from *Dictyostelium discoideum.* Biochim. Biophys. Acta *736*, 45–56.

DeMali, K. A., and Burridge, K. (2003). Coupling membrane protrusion and cell adhesion. J. Cell Sci. *116*, 2389–2397.

Desbarats, L., Brar, S. K., and Siu, C. H. (1994). Involvement of cell-cell adhesion in the expression of the cell cohesion molecule gp80 in *Dictyostelium discoideum.* J. Cell Sci. *107*, 1705–1712.

Dragoi, I. A., and O'Halloran, T. J. (1998). Cloning and characterization of a *Dictyostelium* gene encoding a small GTPase of the Rab11 family. J. Cell. Biochem. *70*, 29–37.

Eisenhaber, B., Bork, P., and Eisenhaber, F. (2001). Post-translational GPI lipid anchor modification of proteins in kingdoms of life: analysis of protein sequence data from complete genomes. Protein Eng. *14*, 17–25.

Eisenhaber, B., Bork, P., Yuan, Y., Loeffler, G., and Eisenhaber, F. (2000). Automated annotation of GPI anchor sites: case study *C. elegans.* Trends Biochem. Sci. *25*, 340–341.

Engqvist-Goldstein, A. E., and Drubin, D. G. (2003). Actin assembly and endocytosis: from yeast to mammals. Annu. Rev. Cell Dev. Biol. *19*, 287–332.

Fang, H., Higa, M., Suzuki, K., Aiba, K., Urushihara, H., and Yanagisawa, K. (1993). Molecular cloning and characterization of two genes encoding gp138, a cell surface glycoprotein involved in the sexual cell fusion of *Dictyostelium discoideum.* Dev. Biol. *156*, 201–208.

Fey, P., Stephens, S., Titus, M. A., and Chisholm, R. L. (2002). SadA, a novel adhesion receptor in *Dictyostelium.* J. Cell Biol. *159*, 1109–1119.

Fukui, Y., Yumura, S., and Yumura, T. K. (1987). Agar-overlay immunofluorescence: high-resolution studies of cytoskeletal components and their changes during chemotaxis. Methods Cell Biol. *28*, 347–356.

Gao, E. N., Shier, P., and Siu, C.-H. (1992). Purification and partial characterization of a cell adhesion molecule (gp150) involved in postaggregation stage cell-cell binding in *Dictyostelium discoideum.* J. Biol. Chem. *267*, 9409–9415.

Harlow, E., and Lane, D. P. (1988). Antibodies: A Laboratory Manual, Cold Spring Harbor, NY: Cold Spring Harbor Laboratory Press.

Hata, T., Takahashi, M., Tanaka, Y., and Urushihara, H. (2001). Total tetra knockout of GP138 multigene family implicated in cell interactions in *Dictyostelium discoideum.* Gene *271*, 33–42.

Hata, T., Yamaguchi, N., Tanaka, Y., and Urushihara, H. (1999). A new member of the GP138 multigene family implicated in cell interactions in *Dictyostelium discoideum.* Cell Struct. Funct. *24*, 123–129.

Hulo, N., Sigrist, C. J., Le Saux, V., Langendijk-Genevaux, P. S., Bordoli, L., Gattiker, A., De Castro, E., Bucher, P., and Bairoch, A. (2004). Recent improvements to the PROSITE database. Nucleic Acids Res. *32*, D134–D137.

Jacquet, M., Guilbaud, R., and Garreau, H. (1988). Sequence analysis of the DdPYR5-6 gene coding for UMP synthase in *Dictyostelium discoideum* and comparison with orotate phosphoribosyl transferases and OMP decarboxylases. Mol. Gen. Genet. *211*, 441–445.

Kessin, R. H. (2001). *Dictyostelium.* Evolution, Cell Biology, and the Development of Multicellularity, New York: Cambridge University Press.

Knecht, D., and Pang, K. M. (1995). Electroporation of *Dictyostelium discoideum.* In: Electroporation Protocols for Microorganisms, vol. 47, ed. J. A. Nickolff, Totowa: Humana Press, 321–330.

Knecht, D. A., Fuller, D. L., and Loomis, W. F. (1987). Surface glycoprotein, gp24, involved in early adhesion of *Dictyostelium discoideum.* Dev. Biol. *121*, 277–283.

Krogh, A., Larsson, B., von Heijne, G., and Sonnhammer, E. L. (2001). Predicting transmembrane protein topology with a hidden Markov model: application to complete genomes. J. Mol. Biol. *305*, 567–580.

Laemmli, U. K. (1970). Cleavage of structural proteins during the assembly of the head of bacteriophage T4. Nature *277*, 680–685.

LaRosa, P. C., Meier, M. B., and Chia, C. P. (2000). A receptor-like glycoprotein from *Dictyostelium discoideum*: functions in phagocytosis and cell adhesion? Mol. Biol. Cell *11*(Suppl.), 554a.

Liu, T., Mirschberger, C., Chooback, L., Arana, Q., Dal Sacco, Z., MacWilliams, H., and Clarke, M. (2002). Altered expression of the 100 kDa subunit of the *Dictyostelium* vacuolar proton pump impairs enzyme assembly, endocytic function and cytosolic pH regulation. J. Cell Sci. *115*, 1907–1918.

Loomis, W. F. (1988). Cell-cell adhesion in *Dictyostelium discoideum.* Dev. Genet. *9*, 549–559.

Lowry, O. H., Rosebrough, N., Farr, A. L., and Randall, R. J. (1951). Protein measurement with the Folin phenol reagent. J. Biol. Chem. *193*, 265–275.

Maniak, M. (2001). Fluid-phase uptake and transit in axenic *Dictyostelium* cells. Biochim. Biophys. Acta *1525*, 197–204.

Marin, F. T., Goyett-Boulay, M., and Rothman, F. G. (1980). Regulation of development in *Dictyostelium discoideum.* III. Carbohydrate-specific intercellular interactions in early development. Dev. Biol. *80*, 301–312.

Maselli, A., Laevsky, G., and Knecht, D. A. (2002). Kinetics of binding, uptake and degradation of live fluorescent (DsRed) bacteria by *Dictyostelium discoideum.* Microbiology *148*, 413–420.

May, R. C., and Machesky, L. M. (2001). Phagocytosis and the actin cytoskeleton. J. Cell Sci. *114*, 1061–1077.

Muller, K., and Gerisch, G. (1978). A specific glycoprotein as the target site of adhesion blocking Fab in aggregating *Dictyostelium* cells. Nature *274*, 445–449.

Myre, M. A., and O'Day, D. H. (2002). Nucleomorphin. A novel, acidic, nuclear calmodulin-binding protein from *Dictyostelium* that regulates nuclear number. J. Biol. Chem. *277*, 19735–19744.

Nakai, K., and Kanehisa, M. (1992). A knowledge base for predicting protein localization sites in eukaryotic cells. Genomics *14*, 897–911.

Nielsen, H., Engelbrect, J., Brunak, S., and von Hejne, G. (1997). Identification of prokaryotic and eukaryotic signal peptides and prediction of their cleavage sites. Protein Eng. *10*, 1–6.

Niewöhner, J., Weber, I., Maniak, M., Mueller-Taubenberger, A., and Gerisch, G. (1997). Talin-null cells of *Dictyostelium* are strongly defective in adhesion to particle and substrate surfaces and slightly impaired in cytokinesis. J. Cell Biol. *138*, 349–361.

Noegel, A., Gerisch, G., Stadler, J., and Westpahl, M. (1986). Complete sequence and transcript regulation of a cell adhesion protein from aggregating *Dictyostelium* cells. EMBO J. *5*, 1473–1476.

Qualmann, B., and Kessels, M. M. (2002). Endocytosis and the cytoskeleton. Int. Rev. Cytol. *220*, 93–144.

Qualmann, B., Kessels, M. M., and Kelly, R. B. (2000). Molecular links between endocytosis and the actin cytoskeleton. J. Cell Biol. *150*, F111–F1116.

Rezabek, B. L., Rodriguez-Paris, J. M., Cardelli, J. A., and Chia, C. P. (1997). Phagosomal proteins of *Dictyostelium discoideum.* J. Euk. Microbiol. *44*, 284–292.

Rivero, F., Furukawa, R., Noegel, A. A., and Fechheimer, M. (1996). *Dictyostelium discoideum* cells lacking the 34,000-dalton actin-binding protein can grow, locomote, and develop, but exhibit defects in regulation of cell structure and movement: a case of partial redundancy. J. Cell Biol. *135*, 965–980.

Sambrook, J., and Russell, D. W. (2001). Molecular Cloning: A Laboratory Manual, Cold Spring Harbor, NY: Cold Spring Harbor Laboratory Press.

Seastone, D. J., Harris, E., Temesvari, L. A., Bear, J. E., Saxe, C. L., and Cardelli, J. (2001). The WASp-like protein scar regulates macropinocytosis, phagocytosis and endosomal membrane flow in *Dictyostelium.* J. Cell Sci. *114*, 2673–2683.

Siu, C. H., Harris, T. J., Wang, J., and Wong, E. (2004). Regulation of cell-cell adhesion during *Dictyostelium* development. Semin. Cell Dev. Biol. *15*, 633–641.

Sussman, M. (1987). Cultivation and synchronous morphogenesis of *Dictyostelium* under controlled experimental conditions. Methods Cell Biol. *28*, 9–29.

Thompson, J. D., Higgins, D. G., and Gibson, T. J. (1994). CLUSTAL W: improving the sensitivity of progressive multiple sequence alignment through sequence weighting, positions-specific gap penalties and weight matrix choice. Nucleic Acids Res. *22*, 4673–4678.

Towbin, H., Staehelin, T., and Gordon, J. (1979). Electrophoretic transfer of proteins from polyacrylamide gels to nitrocellulose sheets: procedure and some applications. Proc. Natl. Acad. Sci. USA *76*, 4350–4354.

Tuxworth, R. I., Weber, I., Wessels, D., Addicks, G. C., Soll, D. R., Gerisch, G., and Titus, M. A. (2001). A role for myosin VII in dynamic cell adhesion. Curr. Biol. *11*, 318–329.

Vogel, G., Thilo, L., Schwarz, H., and Steinhart, R. (1980). Mechanism of phagocytosis in *Dictyostelium discoideum:* phagocytosis is mediated by different recognition sites as disclosed by mutants with altered phagocytotic properties. J. Cell Biol. *86*, 456–465.

Wang, J., Hou, L., Awrey, D., Loomis, W. F., Firtel, R. A., and Siu, C. H. (2000).

The membrane glycoprotein gp150 is encoded by the lagC gene and mediates cell-cell adhesion by heterophilic binding during *Dictyostelium* development. Dev. Biol. *227*, 734–745.

Watts, D. J., and Ashworth, J. A. (1970). Growth of myxamoebae of the cellular slime mold *Dictyostelium discoideum* in axenic culture. Biochem. J. *119*, 171–174.

Wong, E., Yang, C., Wang, J., Fuller, D., Loomis, W. F., and Siu, C. H. (2002). Disruption of the gene encoding the cell adhesion molecule DdCAD-1 leads to aberrant cell sorting and cell-type proportioning during *Dictyostelium* development. Development *129*, 3839–3850.

Yuen, I. S., Jain, R., Bishop, J. D., Lindsey, D. F., Deery, W. J., Van Haastert, P.J.M., and Gomer, R. H. (1995). A density-sensing factor regulates signal transduction in *Dictyostelium*. J. Cell Biol. *129*, 1251–1262.

Zaman, Z., and Verwilghen, R. L. (1979). Quantitation of proteins solubilized in sodium dodecyl sulfate-mercaptoethanol-Tris electrophoresis buffer. Anal. Biochem. *100*, 64–69.

Supplemental Information

Cloning of the gene for gp130 and characteristics of the genomic sequence

We cloned the gene for gp130 using a reverse genetics strategy. The sequences of seven peptides produced by proteolytic cleavage of gel-purified gp130 (schematically indicated in Fig. 1S, panel A) were back-translated to obtain DNA sequence, and degenerate oligonucleotides were designed for use in PCR trials. Because the order of the fragments was unknown, various pairs of primers were tested using different templates in efforts to generate a PCR product containing part of the sequence of gp130. A PCR product encoding two of the sequenced peptides was amplified from a cDNA library (see Materials and Methods below). From this PCR product and the sequence of the partial genomic clone JAX4a237e04 that was identified in a search of databases of the *D. discoideum* Sequencing Consortium, additional primers were designed and subsequently used in primer walking and anchored PCR. The complete cDNA sequence was validated by recovery of a full-length cDNA derived by RT-PCR using primers from the untranslated 5′ and 3′ portions of the composite cDNA and genomic sequences.

The genomic sequence of gp130 is 2472 nucleotides and contains two short introns, one of 68 base pairs (bp), and a second of 97 bp, that are 81 and 91%AT, respectively (Genbank accession AY038935.1), as is typical for *D. discoideum* (Kimmel and Firtel, 1982). The nucleotide sequence data was corroborated when subsequent BLAST searches located the genomic sequence of gp130 in shotgun reads of contigs assigned

initially to chromosome 5 (Welcome Trust Sanger Institute; www.sanger.ac.uk). The recently completed genomic sequence indicates however the sequence of gp130 to be on chromosome 3 (www.dictybase.org). Contig 2608 (9.245 kb) contained and agreed with the gp130 sequence with the exception of small discrepancies in the 5′ non-coding region. Contig 2608 contained non-coding sequences flanking the gene for gp130 that yielded a TATA box, an oligo(dT) stretch, and a presumptive polyadenylation signal, all in positions consistent with the organization of *Dictyostelium* genes (Kimmel and Firtel, 1982). Other BLAST searches revealed portions of the gp130 sequence matched to clones in the vegetative libraries in the Japanese cDNA collection (www.csm.gene.tsukuba.ac.jp/cDNAproject.html; (Morio *et al.*, 1998).

The coding sequence of gp130 (2,307 bases) translates into a preproprotein of 768 amino acids that contains the seven peptides corresponding to microsequenced proteolytic fragments of gel-purified gp130 (Fig. 1A). All were exact matches to the conceptual translation except for an octapeptide sequence reported originally as TLHIPKGE (Chia, 1996) that is instead TLSIPKGE (amino acid residues 503-510). An affinity-purified antibody against the 8-mer synthetic peptide reacted with gp130 (Chia, 1996) and a recombinant form of gp130 produced by expressing a His-tagged fusion protein (Thr151 to Ser759; Supplemental Data, Fig, 1B). This cross-reactivity, and the presence of the other six peptide sequences distributed among the three exons, indicate that the sequenced gene encodes the gp130 protein described previously. Although the octapeptide had a mis-assigned histidine residue and residues IPKG present in all

members of the related gp138 family (see Results), the anti-peptide antibody was specific for gp130 as it did not cross-react with the slower migrating gp138 proteins recognized by a monoclonal antibody (Fig. 1C).

Materials and Methods

Isolation and sequencing of the gene for gp130

Internal amino acid sequences were obtained from gel-purified gp130 proteolyzed with endoproteinase Glu-C as described (Chia, 1996). J. Leszyk (U. Mass. Medical School Core Laboratory for Protein Microsequencing) additionally sequenced peptides derived from trypsinized endo Glu-C fragments. Degenerate oligonucleotides for PCR trials, using *Taq* DNA polymerase (Invitrogen), were designed by back-translation of amino acid sequences. One template, a pACT2 cDNA plasmid library derived from *D. discoideum* strain HL328 (a gift from Dr. Sijie Lu, Baylor College of Medicine, Houston, TX) yielded a PCR product containing two of the sequenced peptides. Concurrently, using the Tblastn routine (Altschul *et al.*, 1990; Altschul *et al.*, 1997), amino acid sequences were used to screen sequences from the Genome Sequencing Centre Jena (Inst. Molecular Biotechnology, Jena, Germany; http://genome.imb-jena.de/dictyostelium). The pUC18 genomic clone JAX4a237e04 (678 bp; sent kindly by G. Glockner) contained an incomplete match to one microsequenced peptide (IGYKNXSFX; residues 228-236) and a perfect match to a second internal peptide (GFILNPSFK; residues 284-292). From the two separate DNA sequences, additional primers were designed and used with the pACT2 cDNA plasmid library in primer walking and anchored PCR that led to the assembly of sequence data covering the entire transcribed cDNA sequence.

The cDNA sequence was validated by recovery of a full-length cDNA derived by RT-PCR using primers from the untranslated 5′ and 3′ portions of the composite cDNA and genomic sequences. With the 5′ and 3′ sequences of the cDNA, a contiguous genomic sequence was assembled from strain Ax3 that spanned the amino acid coding region and contained two introns, with small portions of the flanking 5′ and 3′ non-translated regions. In subsequent BLAST searches of the publicly released databases of the *Dictyostelium* genome project, the genomic sequence of gp130 was found in contigs 2608 (9.245 kb), 5046 (19.263 kb) and recently reported to be on chromosome 3 (contig DDB0203905; www.dictybase.org). Preliminary sequence data were obtained from The Welcome Trust Sanger Institute (www.sanger.ac.uk), Baylor College of Medicine (http://dictygenome.bcm.tmc.edu/), The University of Cologne (http://www.uni-koeln.de) and the Department of Genome Analysis in Jena of the Institute of Molecular Biotechnology (http://genome.imb-jena.de). Nearly all of this data was generated at the aforementioned institutes with a small part of it produced at the Institut Pasteur (http://www.pasteur.fr).

Sequencing of PCR products or plasmids was performed according to the manufacturer's instructions using the ABI 310 and 370A automated sequencers and the ABI PRISM BigDye™ Terminator Cycle Sequencing Ready Reaction Kit (Applied Biosystems; Foster City, CA). Sequences were assembled with Sequencher (Gene Codes).

References

Altschul, S.F., Gish, W., Miller, W., Myers, E.W., and Lipman, D.J. (1990). Basic local alignment search tool. J. Mol. Biol. *215*, 403-410.

Altschul, S.F., Madden, T.L., Schaffer, A.A., Zhang, J., Zhang, Z., Miller, W., and Lipman, D.J. (1997). Gapped BLAST and PSI-BLAST: a new generation of protein database search programs. Nucl. Acids Res. *25*, 3389-3402.

Chia, C.P. (1996). A 130-kDa plasma membrane glycoprotein involved in *Dictyostelium* phagocytosis. Exp. Cell Res. *227*, 182-189.

Kimmel, A.R., and Firtel, R.A. (1982). The organization and expression of the *Dictyostelium* genome. In: The development of *Dictyostelium discoideum*, ed. W.F. Loomis, New York: Academic Press, 234-324.

Morio, T., Urushihara, H., Saito, T., Ugawa, Y., Mizuno, H., Yoshida, M., Yoshino, R., Mitra, B.N., Pi, M., Sato, T., Takemoto, K., Yasukawa, H., Williams, J., Maeda, M., Takeuchi, I., Ochiai, H., and Tanaka, Y. (1998). The *Dictyostelium* developmental cDNA project: generation and analysis of expressed sequence tags from the first-finger stage of development. DNA Res. *5*, 335-340.

Figure Legend-Supplemental Data

Figure S1

Background data that aided in the cloning of the sequence for gp130.

A. Schematic of cloning strategy.

Numbers indicate bases of cloned genomic sequence (GenBank Accession AY038935.1), gray segments represent introns, and black bars above the sequence indicate location of internal peptides from which PCR primers were designed (sequences are underscored in Panel C). An asterisk marks the synthetic 8-mer peptide (TLHIPKGE) used previously to produce an antibody to gp130. JAX4a237e04 (dashed line) is the partial genomic clone acquired from the Jena Sequencing Center, and 13 mer–pACT2 (dashed line) represents a PCR product generated from a pACT2 cDNA library and a reverse primer designed from 13 mer peptide NLLPNQFTDFNEK (residues 432-443 corresponding to bases 1507-1545).

B. Affinity-purified antibody to the synthetic 8-mer recognizes His-tagged recombinant gp130.

Protein blot contains a recombinant version of gp130 (lane 1; 0.25 μg) and plasma membranes from axenically grown (log-phase) Ax2 cells (lane 2; 7.5 μg protein).